

## Excitation of three isospin modes of the giant magnetic dipole resonance in mass 24 isobars\*

R. J. Peterson, F. E. Cecil, and R. A. Ristinen

*Nuclear Physics Laboratory, Department of Physics and Astrophysics, University of Colorado, Boulder, Colorado 80309*

E. R. Flynn, Nelson Stein, and J. D. Sherman

*Los Alamos Scientific Laboratory, Los Alamos, New Mexico 87544*

(Received 29 March 1976)

All three isospin modes of two  $T = 1, 1^+$  states in mass 24 have been studied by ( $^3\text{He}, t$ ), ( $^3\text{He}, ^3\text{He}'$ ), and ( $t, ^3\text{He}$ ) reactions on  $^{24}\text{Mg}$ . The relative strengths of the two  $1^+$  states in each reaction agree with the relative strengths of the electromagnetic transitions, but the shapes and magnitudes of the charge-exchange data are not as predicted by a one-step interaction with a central force. It is necessary to perform a two-step coupled-channel Born-approximation calculation via intermediate  $^4\text{He}$  channels using mixed wave functions to account for the results.

[NUCLEAR REACTIONS  $^{24}\text{Mg}(\beta\text{He}, t)$ , ( $t, ^3\text{He}$ ), ( $^3\text{He}, ^3\text{He}'$ ) to  $1^+$  states. Members of isospin multiplet. Giant  $M1$  states. DWBA, CCBA analysis.]

### I. INTRODUCTION

Mass 3 nuclear projectiles offer access to all three isospin projections of  $T = 1$  excitations. The lowest and most accessible strong isovector excitation in the  $s$ - $d$  shell is the giant magnetic dipole state, which is well known by its large electromagnetic transition rate,<sup>1-3</sup> and which exhausts a large part of the shell model sum rule for the spin-flip  $d_{5/2}$  to  $d_{3/2}$  transition. This strength is found in two  $1^+$  states in  $^{24}\text{Mg}$  at 9.97 and 10.73 MeV. The isobaric analogs of these two states are the 0.47 and 1.35 MeV states<sup>4</sup> of  $^{24}\text{Na}$  ( $T_z = 1$ ) and, as will be shown in this work, the 0.44 and 1.12 MeV states in  $^{24}\text{Al}$  ( $T_z = -1$ ).

The present work reports a complete study of the excitation of all three charge modes of the giant  $M1$  state using  $^3\text{He}$  and triton projectiles. The inelastic scattering of 41.2 MeV  $^3\text{He}$  ions was used to populate the  $T_z = 0$  members; the ( $^3\text{He}, t$ ) reaction at 38.6 MeV was used for the  $T_z = -1$  members; and the ( $t, ^3\text{He}$ ) reaction at 24 MeV was used to study the  $T_z = +1$  members.

The results of these three nuclear reactions may be compared with other magnetic dipole nuclear transitions, such as pion capture,<sup>5</sup> muon capture,<sup>6</sup> and Gamow-Teller  $\beta$  decays,<sup>7</sup> as well as with the well-known damping of static magnetic dipole moments from the Schmidt values.<sup>8</sup> All of these phenomena are related in that they involve nuclear matrix elements of the spin operator  $\sigma$ . The baryonic nuclear reaction allows the study of these nuclear matrix elements at high momentum transfer, and for all three isospin projections.

### II. EXPERIMENTAL PROCEDURE AND RESULTS

The three reactions were studied using highly enriched  $^{24}\text{Mg}$  targets on thin carbon backings. The  $^3\text{He}$  scattering and ( $^3\text{He}, t$ ) reactions were performed with the University of Colorado AVF cyclotron beam and the energy-loss spectrometer.<sup>9</sup> The  $^3\text{He}$  energies were 38.6 MeV for the charge exchange reaction and 41.2 MeV for the inelastic scattering. The reaction products were detected in a helical cathode proportional counter which also measured their positions along the focal plane of the spectrometer. Particle identification was accomplished using the energy loss in the proportional chamber and the residual energy signal from a backing plastic scintillator.<sup>9</sup> The energy resolution was approximately 30 keV, as expected from the first order beam optics of the system. Sample spectra are shown in Figs. 1 and 2. The  $1^+$  states of interest in this work are indicated in each spectrum, except for the  $T = 0, 1^+$  state at 9.83 MeV in  $^{24}\text{Mg}$  which is obscured by the  $^{12}\text{C}$  contaminant at  $7.5^\circ$ . Additional states were also populated and the angular distributions for such states in  $^{24}\text{Al}$  and in  $^{24}\text{Mg}$  will be discussed in future publications.

The ( $t, ^3\text{He}$ ) reaction was studied with the 24 MeV triton beam of the LASL three-stage electrostatic accelerators. The  $^3\text{He}$  ions were analyzed by a Q3D spectrometer, again with the position detection accomplished by a helical cathode proportional counter, with a plastic scintillator to aid the particle identification.<sup>10</sup> A sample spectrum is shown in Fig. 3, with an energy resolution of

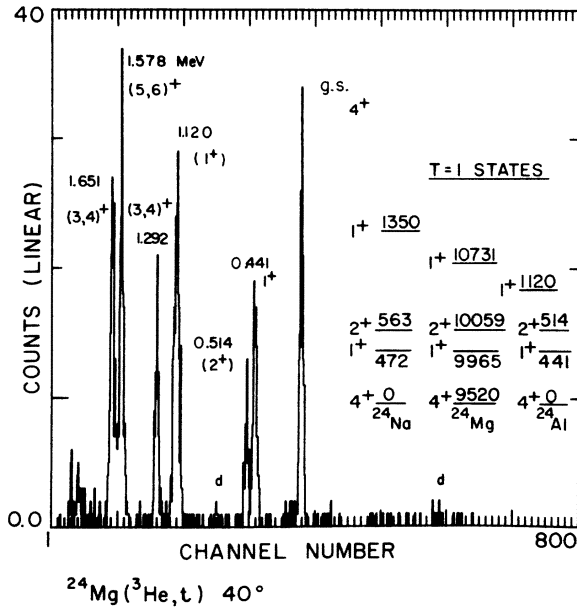


FIG. 1. Momentum spectrum of tritons from the  $^{24}\text{Mg}({}^3\text{He},t)^{24}\text{Al}$  reaction at 38.6 MeV and  $40^\circ$  laboratory angle. Some deuteron peaks which leaked through the particle identification system are labeled "d".

15 keV. The small angle data for the  $(t, {}^3\text{He})$  reaction were obscured by the charge exchange reaction on the hydrogen contamination in the target; this reaction has a large cross section and produces a very broad peak.

The only data other than those for the  $T=1, 1^+$  excitations that are relevant to this report are the cross sections to the  $T=1, 2^+$  states and to the

$T=0, 1^+$  states. These angular distributions are all shown in Figs. 4-6. The 1.347 MeV peak in  $^{24}\text{Na}$  contains a  $1^+$  state but is known to be a multiplet unresolved in the present experiment.<sup>4</sup>

The energy calibration for the  $({}^3\text{He}, t)$  reaction was accomplished by comparison to the prolific deuterons from the  $^{24}\text{Mg}({}^3\text{He}, d)$  reaction<sup>11</sup> to low-lying states of  $^{25}\text{Al}$ , which spanned the same magnetic rigidity range as the tritons of interest. The calibration for the inelastic scattering was accomplished by comparison with the scattering to well known levels of  $^{12}\text{C}$  and  $^{24}\text{Mg}$ . The  $^{24}\text{Mg}(t, {}^3\text{He})^{24}\text{Al}$  reaction proceeds to levels of known energy and spin.<sup>4</sup>

The optical model parameters used to describe the reactions are given in Table I. They were obtained by Rickertsen<sup>12</sup> for mass 3 projectiles on  $^{24}\text{Mg}$  after correcting the observed elastic scattering for the coupled-channel effects due to excitation of the highly collective  $2^+$  state at 1.37 MeV. This parameter set is then appropriate for reactions on the ground state of  $^{24}\text{Mg}$ . Excellent fits to  $({}^3\text{He}, d)$  data on  $^{24}\text{Mg}$  at 38.6 MeV<sup>11</sup> were obtained with this set, which was used for all mass 3 reaction channels.

Since three separate reactions were studied in three experiments at two laboratories, it is necessary to provide a careful normalization among them before any detailed comparisons are justified. The magnitude of the  $({}^3\text{He}, {}^3\text{He}')$  cross sections was measured independently by normalizing to the elastic scattering at small angles using solid state counters. A further check on the magnitude is through the excitation of the 8.358  $T=0, 3^-$  state,

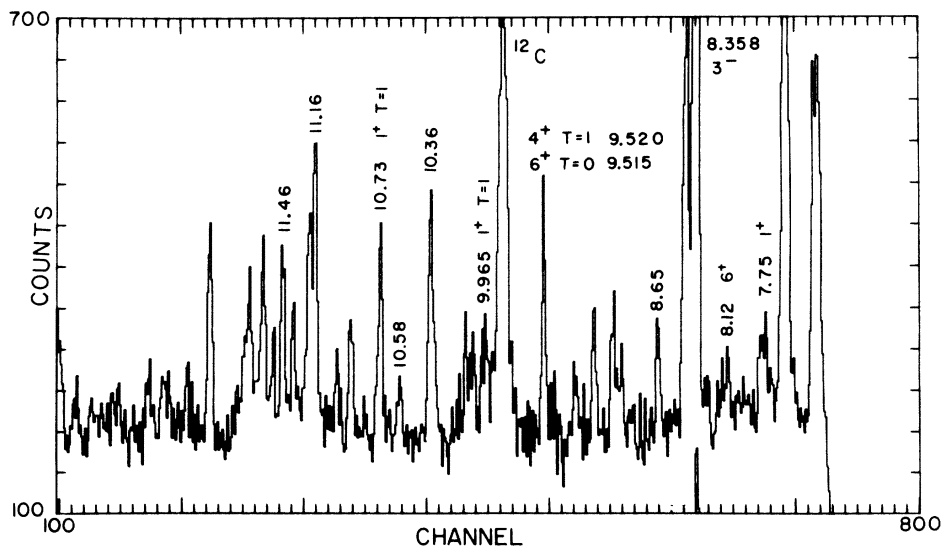


FIG. 2. Momentum spectrum from the inelastic scattering of 41.2 MeV  ${}^3\text{He}$  by  $^{24}\text{Mg}$  at  $7.5^\circ$  laboratory angle. Of the four  $1^+$  states that are relevant to this report, the  $T=0, 1^+$  state at 9.83 MeV is obscured at this angle by a  $^{12}\text{C}$  peak.

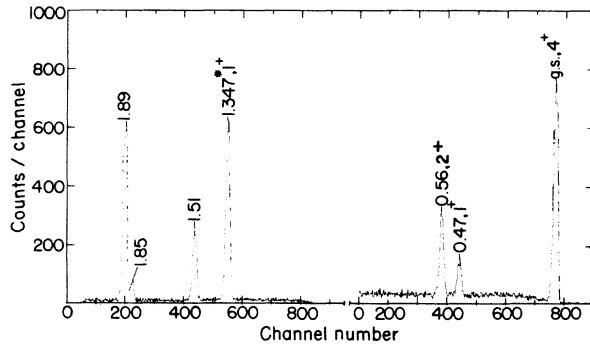


FIG. 3. Momentum spectrum of  ${}^3\text{He}$  from the  ${}^{24}\text{Mg}(t, {}^3\text{He}){}^{24}\text{Na}$  reaction at 24 MeV. The 1.347 MeV peak is known to be a multiplet of states.

observed simultaneously with the  $T=1, 1^+$  states in the spectrometer. The present results provide a value of  $\beta_3$  equal to 0.18, which agrees well with earlier results of  $\alpha$  particle inelastic scattering.<sup>13</sup> The final uncertainty on the cross sections is not greater than  $\pm 15\%$ .

The  $({}^3\text{He}, t)$  cross sections deduced from this normalization are consistent with those for the  $4^+$

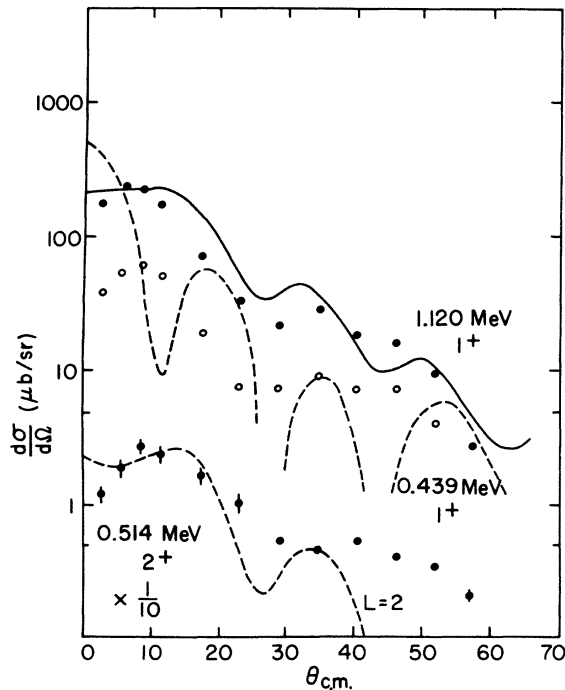


FIG. 4. Angular distributions for the 0.439 ( $1^+$ ), 0.514 ( $2^+$ ), and 1.120 ( $1^+$ ) MeV states of  ${}^{24}\text{Al}$  as observed in the  $({}^3\text{He}, t)$  reaction. The microscopic Yukawa interaction was used with the DWBA to generate the dashed curves for  $L=0$  (upper) and 2, with arbitrary normalization. The solid curve is a DWBA calculation with a collective interaction for  $L=2$ ; this calculation was actually used to generate the ratios  $|\alpha|^2$ , in Table II.

ground state measured previously with semiconductor counters with an uncertainty of 23%.<sup>14</sup> The relative cross sections from the present measurements should be more accurate than the absolute values because the same target was used for both  $({}^3\text{He}, {}^3\text{He}')$  and  $({}^3\text{He}, t)$  reactions. However, this is not certain because the solid angle of the energy-loss spectrometer system is particularly sensitive to the size of the beam spot for the spectrometer conditions used in these experiments. An independent uncertainty of  $\pm 20\%$  is estimated for the absolute normalizations of these data.

The  $(t, {}^3\text{He})$  results from the Q3D spectrometer were normalized to results from a counter-telescope experiment in which both  $(t, {}^3\text{He})$  and triton elastic scattering had been measured simultaneously. The elastic cross sections were extracted by comparison with the optical model at small angles where the predictions are relatively insensitive to the optical model parameters. The estimated error in absolute cross sections is  $\pm 20\%$  for the  $(t, {}^3\text{He})$  data.

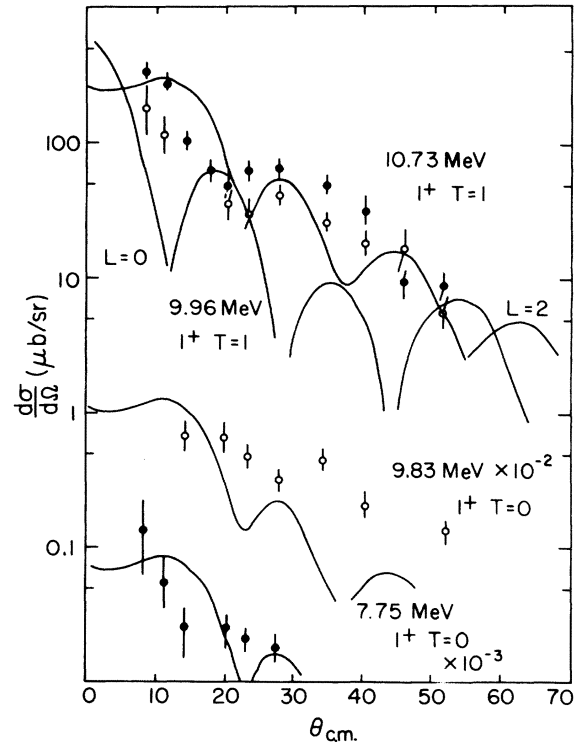


FIG. 5. Inelastic  ${}^3\text{He}$  scattering data to the two  $T=0, 1^+$  states and two  $T=1, 1^+$  states of  ${}^{24}\text{Mg}$ . The curves are DWBA calculations using a collective form factor. The upper two are a comparison of  $L=0$  and  $L=2$  transfers, while the lower two are both  $L=2$ . Just as for the charge exchange reactions, the  $L=2$  curves provide the better fit to the data. Note that the shapes do not depend on the model for the interaction.

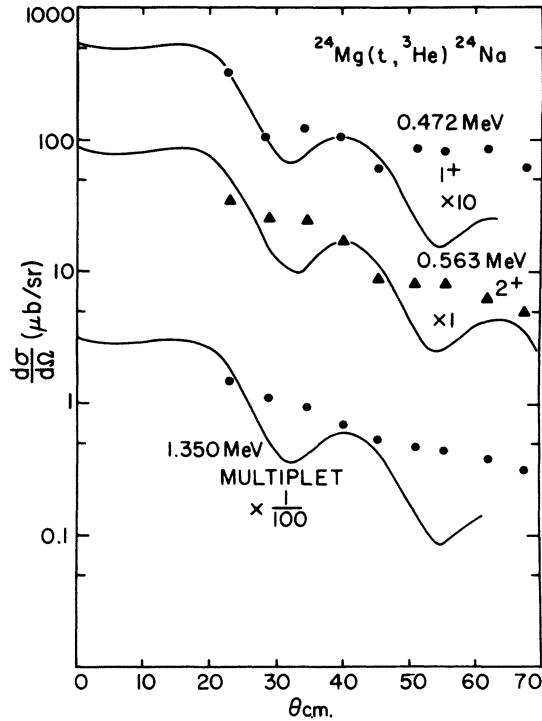


FIG. 6. The charge exchange data to the 0.472 ( $1^+$ ), 0.563 ( $2^+$ ), and 1.35 MeV (multiplet) of  $^{24}\text{Na}$  are compared to DWBA calculations of the collective model  $L=2$  shapes.

### III. DISCUSSION

#### A. Reaction mechanism

##### 1. One-step direct transition

A comparison of the mirror states of  $^{24}\text{Na}$  and  $^{24}\text{Al}$  suggests that the spins of the 0.514 MeV and 1.120 MeV states of  $^{24}\text{Al}$  are  $2^+$  and  $1^+$ , respectively (see Fig. 1), while the level at 0.439 MeV is a known  $1^+$  state. All three of these states exhibit

TABLE I. Optical model parameters used in this work. The first column contains the parameters used for tritons and  $^3\text{He}$ , and the other two columns give the two choices for  $^4\text{He}$  parameters.

	Mass 3 <sup>a</sup>	Shallow $^4\text{He}$ <sup>b</sup>	Deep $^4\text{He}$ <sup>c</sup>
$V$ (MeV)	178.5	47.6	238.0
$r_0$ (fm)	1.104	1.651	1.12
$a$ (fm)	0.722	0.549	0.62
$W_{\text{vol}}$ (MeV)	42	13.8	33.9
$r_0'$ (fm)	1.295	1.651	1.39
$a'$ (fm)	0.852	0.549	0.62
$r_c$ (fm)	1.25	1.25	1.25

<sup>a</sup> References 11, 12.

<sup>b</sup> Reference 13.

<sup>c</sup> Reference 24.

similar shapes in their ( $^3\text{He}, t$ ) angular distributions (see Fig. 4). These similarities reinforce the mirror state argument and also indicate that the principal orbital angular momentum transfer to the  $1^+$  states is  $L=2$ , although both  $L=0$  and  $L=2$  are allowed.

The angular distributions measured for all three reactions to  $1^+$  states are similar in shape at the forward angles, but at other angles they differ somewhat in both shape and magnitudes. The beam energies and  $Q$  values are such that the reactions have roughly the same momentum transfer at each angle. The differences in the reactions have been treated by fitting the observed cross sections to distorted-wave Born-approximation (DWBA) predicted angular distributions using the code DWUCK<sup>15</sup> and assuming a simple collective form factor and an orbital angular momentum transfer  $L=2$ . These predictions are shown on Figs. 4–6. The ratios of experimental to predicted cross sections are labeled  $|\alpha|^2$  and are listed in Table II. These are taken to indicate the strengths

TABLE II. Ratios  $|\alpha|^2$  of observed cross sections to DWBA predictions using a collective model. The quantity  $|\alpha|^2$  represents the strength of a transition with kinematic and  $Q$ -value effects removed so that different reactions may be compared. The ratios of the electromagnetic strengths to the  $T=1$  states of  $^{24}\text{Mg}$  reported as  $2.30 \pm 0.5$  (Ref. 1),  $1.85 \pm 0.15$  (Ref. 2),  $>0.75$  (Ref. 3),  $2.48 \pm 1.3$  (Ref. 18), and  $3.04 \pm 1.0$  (Ref. 32).

Nucleus	$T$	$T_z$	$J^\pi$	Excitation (MeV)	$ \alpha ^2$ ( $\times 10^4$ )	Ratio of $1^+$ states
$^{24}\text{Na}$	1	1	$1^+$	1.35	<62	
			$1^+$	0.47	11 $\pm$ 2.2	<5.6
$^{24}\text{Mg}$	1	0	$1^+$	10.73	24 $\pm$ 4	
			$1^+$	9.97	8.8 $\pm$ 1.3	2.7 $\pm$ 0.4
$^{24}\text{Mg}$	0	0	$1^+$	9.83	17.6 $\pm$ 2.6	
			$1^+$	7.75	8.0 $\pm$ 3.2	3.3 $\pm$ 1.4
$^{24}\text{Al}$	1	-1	$1^+$	1.12	35.2 $\pm$ 7.0	
			$1^+$	0.44	9.42 $\pm$ 1.9	3.7 $\pm$ 0.5

of the transitions. The ratios of the strengths of the two  $1^+$  excitations are listed in each of the four cases of nuclear excitation. The corresponding ratio of the electromagnetic strengths for the 10.73 and 9.97 MeV states of  $^{24}\text{Mg}$  is also given in the table based on several different measurements.

It can be seen in Table II that the ratios of the two  $1^+$  states are approximately the same for each reaction measured in the present work, and that this ratio is also similar to what is observed for the corresponding  $T=1$  electromagnetic transitions. This similarity was the property that first suggested an analogy between the nuclear excitation of  $T=1$ ,  $M1$  states and their excitation by electromagnetic transitions.<sup>16,17</sup> On the other hand, the 9.83 and 7.75 MeV states, both with  $T=0$  and  $1^+$ , are seen very weakly or not at all in the electromagnetic process,<sup>18</sup> which is as expected for an isoscalar  $M1$  transition.<sup>19</sup>

The data from the weak interaction may also be included in the present comparison through the  $\beta$  decay branch of the 0.441 MeV  $1^+$  state of  $^{24}\text{Al}$ .<sup>4</sup> The  $\log ft$  to the  $^{24}\text{Mg}$  ground state is in quite close agreement with the  $B(M1)$  of the analogous electromagnetic transition and thus, a threefold consistency among nuclear, electromagnetic, and  $\beta$  decay transitions is suggested.

The electromagnetic transition rate may be compared to sum rules based on a spherical shell model.<sup>20</sup> In these calculations, the ground state of  $^{24}\text{Mg}$  is assumed to be due to four neutrons  $(1d_{5/2})^4$  and four protons  $(1d_{5/2})^4$  coupled to  $T=0$ , and the excited state is  $(d_{5/2}^7, d_{3/2})$  with  $T=1$ . This predicts a value for the ground state decay width  $\Gamma_0$ , equal to 39.0 eV, while the experimental sum of the two  $1^+$  states yields  $18 \text{ eV}^1$  [for the summed reduced transition rates  $B(M1) = 0.045 \text{ e}^2\text{fm}^2$ ].

If these simple shell model wave functions are assumed for the ground state and  $1^+$  state, then the nuclear excitation is an incoherent sum of  $L=0$  and  $L=2$  terms. Distorted wave calculations using a Yukawa interaction of strength  $V_{\sigma r} = 10 \text{ MeV}$  and range parameter  $\mu = 1.0 \text{ fm}^{-1}$  were made, and the results are shown as the bottom curve in Fig. 7. The  $(^3\text{He}, t)$  reaction is used for this comparison. The  $L=0$  shape dominates the predictions, while the  $L=2$  shape is apparently needed to fit the shape of the data. In addition, the observed  $(^3\text{He}, t)$  cross sections are many times larger than predicted. It is clear therefore that a single-step process, treated microscopically with a central force, is insufficient to understand the data.

The electron and photon scattering data<sup>1</sup> are dominated by the  $L=0$  transfer, as expected for the lower momentum transfer. However, a tensor interaction is also a part of the nuclear excitation

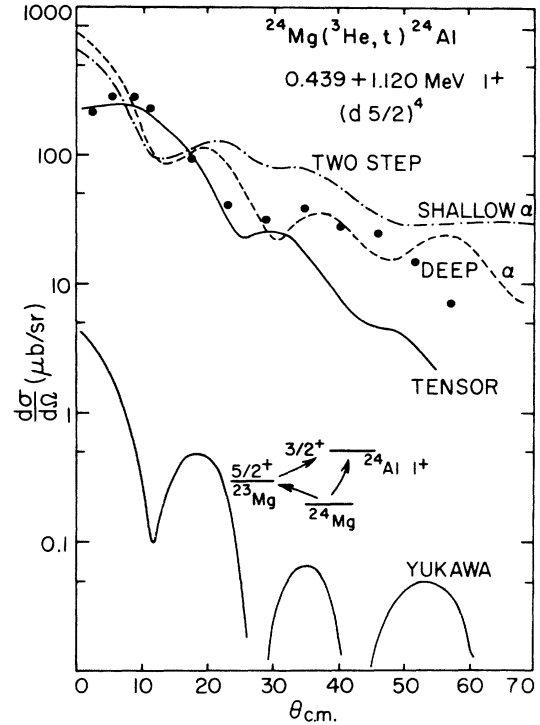


FIG. 7. The summed data from the  $(^3\text{He}, t)$  reaction to the two  $1^+$  states in  $^{24}\text{Al}$  are compared to the microscopic Yukawa prediction ( $V_{\sigma r} = 10 \text{ MeV}$ ,  $\mu = 1.0 \text{ fm}^{-1}$ ); to the tensor prediction ( $V_T = 7 \text{ MeV}$ ,  $\mu = 0.7 \text{ fm}^{-1}$ ); and the two predictions, with different  $\alpha$  particle optical potentials, from the two-step path indicated on the figure. A simple  $(d_{5/2})^4$  configuration for the ground state and  $(d_{5/2}^3 d_{3/2})$  configuration for the  $1^+$  state are assumed.

even though it would have no electromagnetic analog. For transitions to unnatural parity states in  $(^3\text{He}, t)$  reactions, the tensor interaction has been shown to produce larger contributions from the angular momentum transfer of higher  $L$  than from lower  $L$ .<sup>21</sup> The one-pion exchange potential (OPEP) tensor form in DWUCK<sup>15</sup> was used to analyze the present data with  $\mu = 0.7 \text{ fm}^{-1}$  and  $V_T = 7 \text{ MeV}$ . This interaction produces a volume integral larger than the form suggested by Austin and Fox,<sup>22</sup> and is probably an overestimate. The result is shown in Fig. 7 where it can be seen that this interaction and model do indeed account for the shape and magnitude of the data at the forward angles. The standard OPEP form for the tensor interaction has no  $T=0$  term, and hence cannot describe the excitation of the two  $T=0$ ,  $1^+$  states of  $^{24}\text{Mg}$  that are observed in the  $(^3\text{He}, ^3\text{He}')$  reaction with comparable strength as the  $T=1$ ,  $1^+$  states.

## 2. Two-step transition

The third possible excitation mode is by a two-step process  $(^3\text{He}, \alpha)(\alpha, t)$ , through an  $\alpha$  particle

intermediate state. Data on the  $^{24}\text{Mg}(^3\text{He}, \alpha)$  reaction taken simultaneously with the  $(^3\text{He}, t)$  data show the  $5/2^+$  state of  $^{23}\text{Mg}$  at 0.451 MeV to be very strongly excited. The coupled-channel code CHUCK<sup>23</sup> was used to compute the two-step process, with the demand that the intermediate channel cross section be correctly predicted. Following pickup, stripping into an empty  $1d_{3/2}$  shell is assumed, with a spectroscopic strength given by  $(2J_f + 1)S / [(2J_i + 1)(2j + 1)] = \frac{1}{3}$ , where the spectroscopic factor  $S = 1$ . The resulting predictions are shown in Fig. 7 for the two sets of optical model parameters for the  $\alpha$  channel<sup>13,24</sup> listed in Table I. Although this two-step prediction provides the wrong shape, it does predict greater strength than does the direct transfer. Therefore it appears that this mechanism should be pursued with a more sophisticated nuclear model, and the success of the tensor calculation should not be taken for

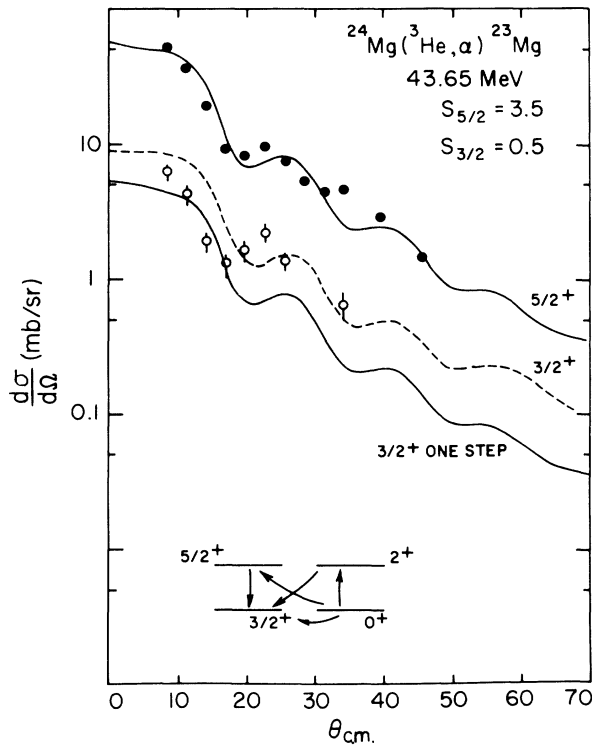


FIG. 8. A comparison of theory with experiment for the  $(^3\text{He}, \alpha)$  reaction to the ground state ( $3/2^+$ ) and 0.451 MeV ( $5/2^+$ ) state of  $^{23}\text{Mg}$ . The solid curves are the one-step DWBA pickup predictions with the spectroscopic factors shown and a value of  $D_0$  (the  $^3\text{He}-\alpha$  overlap) equal to 678. The dashed curve is the prediction for the  $3/2^+$  state when the amplitudes for the inelastic scattering paths shown in the figure are added to the one-step results. A deformation of  $\beta_2 = 0.42$  was used. These data and calculations are for a higher beam energy than used in the  $(^3\text{He}, t)$  reaction, but the predictions and quality of fit are very similar to data at 38.5 MeV.

granted. The two-step yield from  $(^3\text{He}, d)(d, t)$  was also calculated for an intermediate state of a deuteron and  $^{25}\text{Al}$ , but this was found to be a factor of 10 weaker than the  $\alpha$  channel considered above.

If the tensor and two-step paths were comparable in magnitude, then they could coherently interfere so as to produce the observed cross section. However, the calculations indicate that these paths interfere constructively, and hence too large a cross section is predicted.

The two-step model for the  $(^3\text{He}, ^3\text{He}')$  and  $(t, ^3\text{He})$  reactions to  $T = 1$  states should be just the same as for  $(^3\text{He}, t)$ . Moreover, the two-step reaction by  $(^3\text{He}, ^3\text{He}')$  to final  $1^+$  states with  $T = 0$  should be the same as to corresponding  $T = 1$  states by the symmetry of the  $(\alpha, t)$  and  $(\alpha, ^3\text{He})$  reactions on  $^{23}\text{Mg}$ . Experimentally, the two pairs of  $1^+$  states in  $^{24}\text{Mg}$  are excited with similar strength and similar angular distributions, but just as for the  $(^3\text{He}, t)$  and  $(t, ^3\text{He})$  reactions, the two-step theory described above would fail to account for the  $(^3\text{He}, ^3\text{He}')$  reaction as well.

The relative cross sections for exciting various members of isospin multiplets should be independent of the reaction mechanism. Thus the excitation of the  $T = 0$  and  $T = 1$  states of the same configuration with  $T_z = 0$  should be equal by nuclear isospin arguments, and the charge exchange strengths with  $T = 1$ ,  $T_z = \pm 1$  should be twice as large as the analog  $T = 1$ ,  $T_z = 0$  excitation. As far as can be seen in Table II, these predicted relationships are in agreement with the data. However, the poor data for excitation of the 7.75 MeV  $T = 0$ ,  $1^+$  state by inelastic scattering preclude any firm conclusion from its strength.

#### B. Use of wave functions with configuration mixing

Any admixture from the  $1d_{3/2}$  configuration into the ground state which is dominantly  $(1d_{5/2})^8$  has the effect of decreasing  $M1$  matrix elements.<sup>8</sup> This mixing of spin partners is consistent with a supermultiplet scheme, which is at least partially valid in the  $2s-1d$  shell.<sup>25</sup> The influence of this mixing on the reaction data will now be investigated.

The neutron pickup reactions<sup>26</sup> on  $^{24}\text{Mg}$  find some  $d_{3/2}$  strength, suggesting a model ground state for neutrons of the form

$$0.75(d_{5/2})^4 + 0.25(d_{5/2})^2(d_{3/2})^2.$$

The positive sign is consistent with a pairing interaction. Very little  $2s_{1/2}$  strength is found in the pickup reaction<sup>26</sup> on  $^{24}\text{Mg}$ .

The validity of this ground state may be tested by computing the reduced matrix elements and summing over the 10.73 and 9.97 MeV  $1^+$  states of

$^{24}\text{Mg}$ . This provides  $B(M1) = 3.91 \times 10^{-2} e^2\text{fm}^2$ , compared to the measured value<sup>1</sup> of  $(4.49 \pm 0.52) \times 10^{-2} e^2\text{fm}^2$ . Using the mixed ground state wave function, DWBA calculations were performed with the same central and tensor forces as for the pure ground state. The final state in the calculations was taken as  $1^+$  with the  $(d_{5/2}^3 d_{3/2})$  configuration. It was expressly kept simple to avoid introducing more parameters than are absolutely necessary. The results are shown as the two lower curves in Fig. 9. Both predictions are strongly decreased due to the mixed ground state.

A failure of the model wave function given above is that it predicts pickup cross sections to  $^{23}\text{Mg}$  that do not agree with the data. The predicted values are  $S_{5/2} = 3.5$ ,  $S_{3/2} = 0.5$ , while the present data and previous<sup>26</sup> data indicate values near 4.0 and 2.0. For the expected weak  $\frac{3}{2}^+$  state, two-step contributions are important. The data and two-step paths are sketched in Fig. 8. The amplitudes from the two two-step paths add coherently when the inelastic scattering is described by the collective rotational model. The  $d_{5/2}$  pickup from the  $2^+$  state and the inelastic scattering from the  $\frac{5}{2}^+$  to the  $\frac{3}{2}^+$  states are both proportional to the same geometric term  $(\frac{5}{2} \frac{3}{2} 2 0 | \frac{3}{2} \frac{3}{2})^2$ .

The direct one-step pickup predictions for  $^{24}\text{Mg}(^3\text{He}, \alpha)$  to the  $\frac{5}{2}^+$  and  $\frac{3}{2}^+$  states are shown in Fig. 8. When both the two-step and one-step amplitudes to the  $\frac{3}{2}^+$  state are added, the dashed curve is obtained. Thus the calculations including two-step contributions, when extended properly to second order, seem to provide a better description of the  $(^3\text{He}, \alpha)$  data.

Rather than include these paths explicitly in the two-step  $(^3\text{He}, t)$  analysis, a spectroscopic factor is used for  $S_{3/2}$  that predicts correctly the observed yield to the  $\frac{3}{2}^+$  state. Note that pickup to the  $\frac{5}{2}^+$  state is adequately described already by a one-step process. The proton stripping is taken to be into  $d_{5/2}$  or  $d_{3/2}$  orbits as left empty by the model wave function. The spectroscopic amplitude for the stripping of a  $d_{3/2}$  particle onto the  $\frac{5}{2}^+$  state of  $^{23}\text{Mg}$  is simply

$$\frac{1}{8} [1 - \frac{1}{4}(0.5)]^{1/2}.$$

Included in Fig. 9 are the  $(^3\text{He}, t)$  data and the two-step prediction by intermediate nucleon transfer. The data are seen to be successfully predicted at forward angles, in both shape and magnitude, without free parameters. The coherent addition of the tensor or Yukawa amplitudes has little effect on the predicted shape. At larger angles there is disagreement, but as shown in Fig. 7, the choice of the  $\alpha$  particle optical potential has a stronger effect on those data than the forward angle data, and for present purposes it seemed undesirable

to vary these parameters.

The mixed ground state configuration shown above permits several  $1^+$  excitations in addition to the  $(d_{5/2}^3, d_{3/2})$  used in the calculations. These include the  $(d_{5/2}, d_{3/2}^3)$  and the  $(d_{5/2}^2, d_{3/2}, s_{1/2})$ , the latter being formed by promotion into the  $2s$  shell. Energy systematics suggest that the  $d_{3/2}$  orbital lies quite high in excitation and in the present analysis the  $(d_{5/2}, d_{3/2}^3)$  configuration is ignored. On the other hand, even though the transition involving the  $s_{1/2}$  orbital is forbidden in the electromagnetic case which involves only spin-orbit partners, the fact that the  $M1$  giant resonance is split into two  $1^+$  states<sup>3</sup> indicates a mixture of configurations.

Calculations including the  $(d_{5/2}^2 d_{3/2} s_{1/2})_{1^+}$  configuration are shown in Fig. 10. The lower curve is the result of the two-step transition to this configuration alone starting from the mixed ground state given above. The prediction lies far below the experimental data in magnitude. To obtain the upper curve, transitions from the mixed ground state to both the  $(d_{5/2}^3 d_{3/2})_{1^+}$  and  $(d_{5/2}^2 d_{3/2} s_{1/2})_{1^+}$  configurations are summed, and the result is compared with the sum of the experimental cross sec-

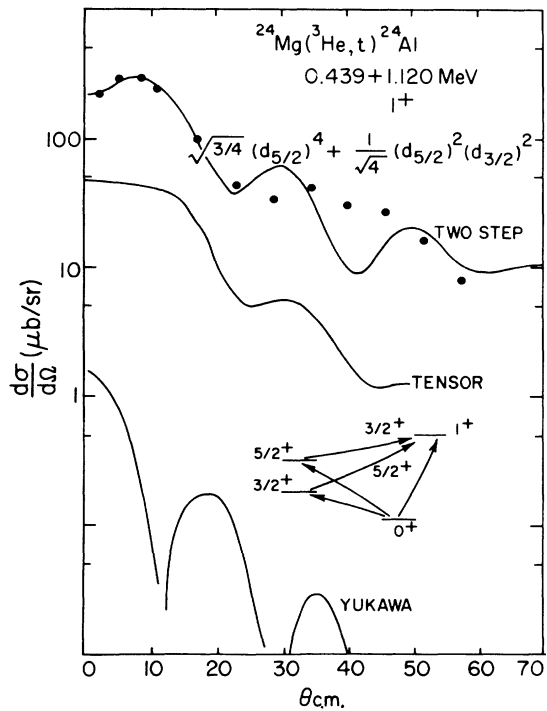


FIG. 9. The same data as in Fig. 7, but a mixed ground state configuration is now assumed in the calculations. The parameters are the same as used in the calculations of Fig. 7, except that only the family with the deep potential is used for the  $^4\text{He}$  channel. Note that the Yukawa and tensor results are reduced in strength compared with Fig. 7, while the two-step prediction is dramatically changed in shape.

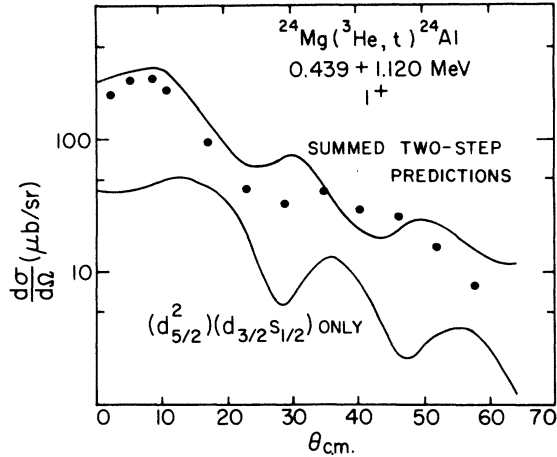


FIG. 10. The lower curve is a two-step calculation from the mixed ground state to a  $1^+$  state with the configuration  $(d_{5/2}^2 d_{3/2} s_{1/2})$ . The upper curve is the summed prediction to two  $1^+$  states with configurations of  $(d_{5/2}^2 d_{3/2})$  and  $(d_{5/2}^2 d_{3/2} s_{1/2})$ . The data are the summed cross sections for the two  $1^+$  states, as originally shown in Fig. 7.

tions to the two  $1^+$  states. As can be seen in Fig. 10, the agreement is only slightly worse than in Fig. 9.

The spherical shell model admittedly may pro-

vide a poor basis for describing a nucleus as deformed as  $^{24}\text{Mg}$ . However, calculations were also performed using the Nilsson scheme, and all of the same features dominate the results as in the spherical scheme. Thus the  $B(M1)$  is reduced; the configuration mixing in the ground states provides destructive interference in the two-step calculation which reduces the predicted  $(^3\text{He}, t)$  cross section to the correct magnitude; and the shape of the angular distribution is also correctly predicted to take on the  $L = 2$  character.

### C. Influence of strong absorption

The comparison of baryonic and electromagnetic excitation of the  $1^+$  states in the  $s$ - $d$  shell was first made using the ratios of strengths to states in the same nucleus.<sup>16,17</sup> For  $^{24}\text{Mg}$ , the various ratios are listed in Table II. The correspondence is more obvious for  $^{28}\text{Si}$ , where five  $1^+$  states are seen in the electron scattering<sup>28</sup> and  $(t, ^3\text{He})$  reactions,<sup>17</sup> and at least three in the  $(^3\text{He}, t)$ <sup>29</sup> reaction. Again, the ratios are quite similar.

It now remains to explain why these ratios are similar, since the electromagnetic interaction is proportional only to a nuclear matrix element of  $\sigma\tau$ , while the  $(t, ^3\text{He})$ ,  $(^3\text{He}, ^3\text{He}')$ , and  $(^3\text{He}, t)$  reactions may proceed both by this process and ad-

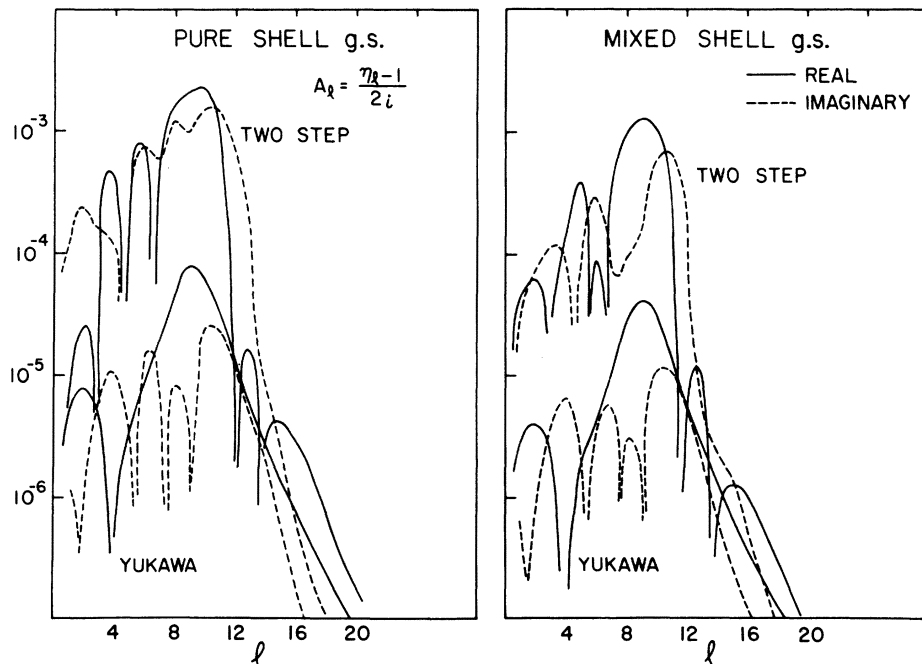


FIG. 11. The scattering amplitudes are shown for each partial wave, with  $J = l$ , for the two-step prediction and the one-step Yukawa interaction prediction. The real amplitudes are solid curves and the imaginary are dashed. The signs of the amplitudes are the same at the peak, near the classical grazing incidence. The left half of the figure shows the amplitudes for the predictions of Fig. 7; the right half, for the predictions of Fig. 9. The results for  $J = l \pm 1$  are very similar.



ditional complex two-step processes.

One possible approach may be to examine the scattering amplitudes in the  $S$ -matrix description of the reaction. The  $S$ -matrix elements are plotted in Fig. 11 for the two-step and the Yukawa predictions based on the shell model wave functions discussed in Sec. III and Sec. IV. The Yukawa amplitudes represent a one-body matrix element of  $\sigma\tau$ , and should provide cross sections proportional to the electromagnetic reduced matrix elements.

It is noted that the Yukawa amplitudes are much smaller than the two-step amplitudes but, aside from their absolute magnitudes, they appear to be similar in other respects. Thus, at the maximum of real and imaginary values, they have the same relative signs and the same ratio of real to imaginary. They peak at the same  $l$ , near the classical grazing incidence, and their general shapes are quite similar. Only the results for  $J=l$  are shown, but the same results are found for  $J=l\pm 1$ . It is thus not surprising to find approximate proportionality between the one- and two-step mechanisms. This is true primarily because of the strong absorption, since for smaller impact parameters, major differences are noted for the two-reaction processes. For the present case, the smaller impact parameters have little influence due to the smaller amplitudes. Also, it should be noted that the two-step elements decrease more rapidly than the one-step at large impact parameters. This would be expected if two nuclear interactions must occur in the region of very low nucleon density.

It has been shown that the interference from mixed configurations produces a larger cancellation of the  $L=0$  cross section than the  $L=2$  cross section for  $1^+$  states, which agrees with the experimental data. This result may be attributed to the sharp peaking of the  $S$ -matrix elements in  $l$  space. When only one grazing partial wave  $L$  is responsible for the reaction, one finds simplifications in the expression for the differential cross section. In the notation of Tobocman and Satchler,<sup>30</sup> the transition matrix elements are written as

$$\beta_{SJ}^{Lm} = \sum_{L_a, L_b} \Gamma_{L_b L_a}^{Lm} P_{L_b}^m(\theta) f_{L_a L_b}^L,$$

where the  $\Gamma_{L_b L_a}^{Lm}$  contains the triangle condition ( $\begin{smallmatrix} L_a & L_b & L \\ 0 & 0 & 0 \end{smallmatrix}$ ). If only  $L_b=L$  is nonzero, then there is only one term in this sum for  $L=0$ , but five for  $L=2$ . It is clearly easier to obtain strong cancellation for the single  $L=0$  term than for a more complex expression for  $L=2$  containing many terms.

The suggested two-step reaction mechanism provides large differences in polarization of the outgoing projectile depending on whether a mixed or

pure shell model ground state wave function is used. The tensor interaction yields a polarization different from both of these, and essentially independent of the details of the ground state.

#### IV. SUMMARY

Charge exchange and inelastic scattering by mass 3 projectiles to the  $1^+$  states of the mass 24 nuclei show angular distributions which are quite similar. Moreover, the relative strengths of the charge exchange and the inelastic transitions with  $T=1$  to corresponding states are in agreement with isospin coupling rules. There is also a similarity between the ratios of strengths to the two  $1^+$  states excited by nuclear reactions and the electromagnetic intensity ratio. Thus the experimental results discussed here are consistent with the excitation of the three isospin modes of the  $T=1$  giant  $M1$  resonance. A detailed examination of the differential cross sections reveals, however, that the actual mechanism of excitation of these modes is quite complicated. In particular, the present analysis shows that a two-step reaction of sequential pickup and stripping appears to be favored over the direct excitation. If only direct excitation is used, then a tensor force is required to describe the observed shapes of the distributions, in contrast to the electromagnetic transitions. Moreover, a strong mixing between  $d_{5/2}$  and  $d_{3/2}$  orbits in the ground state of  $^{24}\text{Mg}$  is required to bring the observed strengths into agreement with the electromagnetic results. It is suggested that the strong absorption characteristics of the mass 3 particles cause a qualitative similarity between the scattering amplitudes of the complex two-step processes and the single-step reaction. This result may well be responsible for the observed similarity between nuclear reaction data on the one hand, and  $M1$  electromagnetic transitions and Gamow-Teller  $\beta$  decay on the other.

For the simplest mixture of  $d_{5/2}$  and  $d_{3/2}$  wave functions in the ground state of  $^{24}\text{Mg}$ , four important experimental results are reproduced. These are the  $B(M1)$  to the giant magnetic dipole state,<sup>1-3</sup> the pickup to the states of  $^{23}\text{Mg}$  (with an additional two-step mechanism added to obtain this), and both the magnitude and shape of the  $(^3\text{He}, t)$  data. The observed existence of two  $1^+$  states is predicted by the Nilsson scheme and can be accommodated in the spherical shell model.

Another nuclear reaction that has been used to populate  $1^+$  states is  $(^6\text{Li}, ^6\text{He})$ .<sup>31</sup> The data show several features also found in the present work: larger cross sections than predicted by a microscopic one-step process, and angular distributions with  $L=2$  shapes for  $1^+$  final states. The presently

reported reactions allow fairly simple interpretations that may not be feasible with the more complicated ( ${}^6\text{Li}$ ,  ${}^6\text{He}$ ) case.

The present results suggest that the hadronic reactions ( ${}^3\text{He}$ ,  $t$ ), ( ${}^3\text{He}$ ,  ${}^3\text{He}'$ ), and ( $t$ ,  ${}^3\text{He}$ ) all belong to the family of nuclear processes that are related through a common isovector "spin-flip" matrix

element. Thus the influence of the supermultiplet symmetry appears to be extended yet further to the complex process of two-step nuclear reactions at high momentum transfer.

Many useful insights regarding this work resulted from discussions with A. Bohr and P. D. Kunz.

\*Work supported in part by the U.S. Energy Research and Development Administration.

<sup>1</sup>A. Johnston and T. E. Drake, *J. Phys.* **A7**, 898 (1974).

<sup>2</sup>L. W. Fagg, W. L. Bendel, S. K. Numrich, and B. T. Chertok, *Phys. Rev.* **163**, 1278 (1967).

<sup>3</sup>H. W. Kuehne, P. Axel, and D. C. Sutton, *Phys. Rev.* **163**, 1278 (1967).

<sup>4</sup>P. M. Endt and C. Van der Leun, *Nucl. Phys.* **A214**, (1973).

<sup>5</sup>M. Ericson and M. Rho, *Phys. Rep.* **5C**, 58 (1972).

<sup>6</sup>J. D. Walecka, in *Muon Physics*, edited by C. S. Wu and V. W. Hughes (to be published).

<sup>7</sup>A. Arima and H. Horie, *Prog. Theor. Phys.* **12**, 623 (1954).

<sup>8</sup>A. Bohr and B. R. Mottelson, *Nuclear Structure* (Benjamin, New York, 1969), Vol. 1, p. 336.

<sup>9</sup>B. W. Ridley *et al.*, *Nucl. Instrum. Methods* **130**, 79 (1975).

<sup>10</sup>E. R. Flynn, S. Orbesen, J. D. Sherman, J. W. Sunier, and R. Woods, *Nucl. Instrum. Methods.* **128**, 35 (1975).

<sup>11</sup>R. J. Peterson and R. A. Ristinen, *Nucl. Phys.* **A246**, 402 (1975).

<sup>12</sup>L. D. Rickertsen (private communication).

<sup>13</sup>T. M. Nagib and J. S. Blair, *Phys. Rev.* **165**, 1250 (1968).

<sup>14</sup>N. Mangelson, M. Reed, C. C. Lu, and F. Ajzenberg-Selove, *Phys. Lett.* **21**, 661 (1966).

<sup>15</sup>DWUCK, a distorted-wave Born-approximation code written by P. D. Kunz, University of Colorado (unpublished).

<sup>16</sup>E. R. Flynn, J. D. Garrett, and N. Stein, in *Proceedings of the International Conference on Nuclear Physics, Munich, 1973*, edited by J. de Boer and H. J. Mang (North-Holland, Amsterdam/American Elsevier, New

York, 1973), Vol. I, p. 650.

<sup>17</sup>E. R. Flynn, J. Sherman, and N. Stein, *Phys. Rev. Lett.* **32**, 846 (1974).

<sup>18</sup>U. E. P. Berg, K. Wienhard, and H. Wolf, *Phys. Rev. C* **11**, 1851 (1975).

<sup>19</sup>G. Morpurgo, *Phys. Rev.* **110**, 721 (1958).

<sup>20</sup>D. Kurath, *Phys. Rev.* **130**, 1525 (1963).

<sup>21</sup>E. Rost and P. D. Kunz, *Phys. Lett.* **30B**, 231 (1969).

<sup>22</sup>S. M. Austin and S. H. Fox, in *Proceedings of the International Conference on Nuclear Physics, Munich, 1973* (see Ref. 16), p. 388.

<sup>23</sup>CHUCK, a coupled-channel code written by P. D. Kunz, University of Colorado (unpublished).

<sup>24</sup>The deep  ${}^4\text{He}$  potential was modified from the parameters of P. P. Singh, R. E. Malmin, M. High, and D. W. Devins, *Phys. Rev. Lett.* **23**, 1124 (1969), so as to match the radius parameter for both the ingoing and outgoing projectile.

<sup>25</sup>J. B. McGrory, *Phys. Lett.* **33B**, 327 (1970); N. C. Mukhopadhyay and F. Cannata, *ibid.* **51B**, 225 (1974).

<sup>26</sup>R. O. Nelson and N. R. Roberson, *Phys. Rev. C* **6**, 2153 (1972); R. L. Kozub, *Phys. Rev.* **172**, 1078 (1968).

<sup>27</sup>S. G. Nilsson, *K. Dan. Vidensk. Selsk. Mat-Fys. Medd.* **29**, No. 16 (1955).

<sup>28</sup>L. W. Fagg, W. L. Bendel, E. C. Jones, Jr., and S. Numrich, *Phys. Rev.* **187**, 1378 (1969).

<sup>29</sup>R. J. Peterson *et al.* (unpublished).

<sup>30</sup>W. Toboeman and G. R. Satchler, *Phys. Rev.* **118**, 1566 (1960); R. H. Bassel, R. M. Drisko, and G. R. Satchler, Oak Ridge National Laboratory Report No. ORNL-3240, 1962 (unpublished).

<sup>31</sup>W. R. Wharton and P. T. Debevec, *Phys. Lett.* **51B**, 447, 451 (1974).

<sup>32</sup>O. Titze, *Z. Phys.* **220**, 66 (1969).